The effect of molnupiravir and nirmatrelvir on SARS-CoV-2 genome diversity in infected and immune suppressed mice.

Rebekah Penrice-Randal[1*†], Eleanor G. Bentley[1*], Parul Sharma[1], Adam Kirby[1], I'ah Donovan-Banfield[1,2], Anja Kipar[1,3], Daniele F. Mega[1] Chloe Bramwell[1,4], Joanne Sharp[4], Andrew Owen[4,5], Julian A. Hiscox[1,2,6] and James P. Stewart[1,5].

[1]Department of Infection Biology and Microbiomes, University of Liverpool, Liverpool, UK.
[2]NIHR Health Protection Research Unit in Emerging and Zoonotic Infections, Liverpool, UK.
[3]Laboratory for Animal Model Pathology, Institute of Veterinary Pathology, Vetsuisse Faculty, University of Zurich, Switzerland.
[4]Department of Pharmacology and Therapeutics, University of Liverpool, UK.
[5]Centre of Excellence in Long-acting Therapeutics (CELT), University of Liverpool, UK.
[6]A*STAR Infectious Diseases Laboratories (A*STAR ID Labs), Agency for Science, Technology and Research (A*STAR), Singapore.

*These authors contributed equally.
† Corresponding author: rebee@liverpool.ac.uk

Running title: Antiviral and SARS-CoV-2 genome diversity

Synopsis

Objectives. Immunocompromised individuals are susceptible to severe COVID-19 and potentially contribute to the emergence of variants with altered pathogenicity due to persistent infection. This study investigated the impact of immunosuppression on SARS-CoV-2 infection in k18-hACE2 mice and the effectiveness of antiviral treatments in this context.

Methods Mice were immunosuppressed using cyclophosphamide and infected with a B lineage of SARS-CoV-2. Molnupiravir and nirmatrelvir, alone and in combination, were administered and viral load and viral sequence diversity was assessed.

Results Treatment of infected but immune compromised mice with both compounds either singly or in combination resulted in decreased viral loads and pathological changes compared to untreated animals. Treatment also abrogated infection of neuronal tissue. However, no consistent changes in the viral consensus sequence were observed, except for the emergence of the S:H655Y mutation. Molnupiravir, but not nirmatrelvir or immunosuppression alone, increased the transition/transversion (Ts/Tv) ratio, representative of A>G and C>U mutations and this increase was not altered by the co-administration of nirmatrelvir with molnupiravir.

Notably, immunosuppression itself did not appear to promote the emergence of mutational characteristic of variants of concern (VOCs).

Conclusions Further investigations are warranted to fully understand the role of immunocompromised individuals in VOC development and to inform optimised public health strategies. It is more likely that immunodeficiency promotes viral persistence but does not necessarily lead to substantial consensus-level changes in the absence of antiviral selection pressure. Consistent with mechanisms of action, molnupiravir showed a stronger mutagenic effect than nirmatrelvir in this model.

Keywords

SARS-CoV-2, COVID-19, immunocompromised, intra-host evolution, Molnupiravir, Nirmatrelvir, Paxlovid.

Introduction

Unsurprisingly, since the start of the SARS-CoV-2 pandemic and the first deposited genome sequences, and like other coronaviruses, SARS-CoV-2 has diverged through single nucleotide polymorphism, and homologous and heterologous recombination applications resulting in insertions and deletions [1, 2]. Over the course of the pandemic changes that have dominated have resulted in increased transmissibility such as the P323L/D614G changes in early 2020 [3-5], immune-evasion [6] and altered pathogenicity [7].

Founder effects, population bottlenecks, selection pressures and behaviour have contributed to the diversification of the SARS-CoV-2 genome but also to the apparent waves of different variants. Several Variants of Concern (VoCs) have arisen that have a transmission advantage and/or potential immune evasion. Some reports have suggested that such variants may have arisen in hosts with compromised immunity and/or persistent infections, where infection leads to the generation of more diverse variants through longer viral evolution within an individual [8]. This includes a changing landscape of dominant viral genome sequence and minor genomic variants in immune compromised individuals e.g. in a patient with cancer [9]. Changes within the individual mapped to several different regions on the SARS-CoV-2 genome including the spike glycoprotein and orf8.

Complicating the picture of potential rapid and dramatic genomic change in immune compromised hosts is that similar changes can be observed in immune competent patients. This can be either as part of the dominant genomic sequence [10] or minor variant genomes [1]. Indeed, genomic variants with deletions can be identified in the minor genomic variant population of Middle East respiratory syndrome coronavirus (MERS-CoV) from patients [11] and as part of the dominant genomic sequence in camels [12, 13].

Parallels with other animal coronaviruses can be found where persistent infections are established, and this might be associated in pathogenicity; an example are feline coronavirus (FCoV) infections and feline infectious peritonitis (FIP) [14-17]. Thus, one

concern with long term persistence of SARS-CoV-2 in immune compromised patients is that new transmissible variants could emerge [8].

Three small molecule direct acting anti-virals (DAAs) have received early use authorisation for the treatment of COVID-19: remdesivir, molnupiravir (both nucleoside analogues which target viral nucleic acid synthesis) and nirmatrelvir (which targets the main viral protease). Unlike remdesivir, molnupiravir and nirmatrelvir are orally administered and thus more readily deployed for treatment in the community. Nirmatrelvir is packaged with ritonavir (as Paxlovid), this later molecule acting as a pharmacokinetic boosting agent to inhibit P450 (CYP) 3A4. However, adequate nirmatrelvir plasma concentrations can be achieved in mice without the need for ritonavir boosting. In cell culture single or combination treatment can result in decreased viral replication [18, 19] and a natural extension is that such anti-virals may be deployed as combination therapy to reduce the emergence of resistant genotypes [20]. Resistant genotypes/phenotypes have been identified in vitro for remdesivir [21]. Molnupiravir has previously been shown to enhance viral transition/transversion mutations in a phase II clinical trial [22] and a molnupiravir associated signature has been identified in circulating SARS-CoV-2 lineages since the introduction of molnupiravir in 2022 [23].

Immunocompromised patients with a SARS-CoV-2 infection are treated as a priority with anti-virals, including those compounds that generically target virus replication by causing hyper-mutation or specifically preventing the function of a viral protein critical to the life cycle of the virus. Such anti-virals may be deployed as combination therapy to reduce the emergence of resistant genotypes [20] and may be particularly relevant for patients with compromised immunity [24]. However, in the latter patients, anti-virals may decrease viral loads but enhance genomic plasticity. To investigate this, the genomic variation of SARS-CoV-2 was evaluated in an immune compromised host, in the absence and presence of medical countermeasures. We have developed animal models of COVID-19 to be able to assess pathogenicity of new variants and develop interventions [25-27]. An immune suppressed K18-hACE2 transgenic mouse model was used to simulate patients with severe COVID-19 [28, 29]. Two anti-virals, molnupiravir and nirmatrelvir, were evaluated either singly or in combination.

Methods

Animal infection and treatment

A UK variant of SARS-CoV-2 (hCoV-2/human/Liverpool/REMRQ0001/2020), was used as described previously [30, 31].

Animal work was approved by the local University of Liverpool Animal Welfare and Ethical Review Body and performed under UK Home Office Project Licence PP4715265. Transgenic mice carrying the human ACE2 gene under the control of the keratin 18 promoter (K18-hACE2; formally B6.Cg-Tg(K18-ACE2)2Prlmn/J) were purchased from Jackson Laboratories (France) at 8 – 10 weeks of age. Mice were maintained under SPF barrier conditions in individually ventilated cages and underwent a week of acclimatisation in these conditions prior to experimental use.

Experimental design is shown in Fig. 1 and treatment groups detailed in Table 1. Animals were randomly assigned into multiple cohorts of four animals using a random number generator. For operational reasons at high containment the treatment groups were not blinded during the experiment. Sample size was determined using prior experience of similar experiments with SARS-CoV-2. For SARS-CoV-2 infection, mice were anaesthetized lightly with isoflurane and inoculated intra-nasally with 50 µl containing 10^4 PFU SARS-CoV-2 in PBS as described previously [26]. Some cohorts of mice were immunosuppressed by treatment with cyclophosphamide (100 mg/kg) intra-peritoneally (IP) at day -4 and -1 pre-infection. Molnupiravir was made up in 10% PEG400 and 2.5% cremophor in water and used at 100 mg/kg. Nirmatrelvir was dissolved in 2% Tween 80 in 98% (v/v) of 0.5% methyl cellulose and used at 500 mg/kg. Both drugs were administered via the oral route one hour prior to infection and then twice daily up to 4 days post-infection via the oral (PO) route. Groups of animals were kept in the same cages during the experiment and were always weighed and treated in the same order. Mice were sacrificed at day 6 (vehicle and cyclophosphamide treated group) or 7 (all others) after infection by an overdose of pentobarbitone. Weights were recorded daily, and tissues were removed immediately for downstream processing. The right lung and nasal turbinates were frozen at -80 °C until further processing. The left lung and heads were fixed in 10% neutral buffered formalin for 24-48 h and then stored in 70%. No data were excluded from the analyses.

Histology, immunohistology and morphometric analysis

The fixed left lung was routinely paraffin wax embedded. Heads were sawn longitudinally in the midline using a diamond saw (Exakt 300; Exakt) and the brain left in the skull. Heads were gently decalcified in RDF (Biosystems) for twice 5 days, at room temperature and on a shaker, then both halves paraffin wax embedded. Consecutive sections (3-5 µm) were either stained with hematoxylin and eosin (HE) or used for immunohistology (IH). IH was performed to detect viral antigen expression using the horseradish peroxidase method and a rabbit anti-SARS-CoV nucleocapsid protein (Rockland, 200-402-A50) as primary antibody, as previously described [26, 32, 33].

For morphometric analysis, the immunostained sections were scanned (NanoZoomer-XR C12000; Hamamatsu, Hamamatsu City, Japan) and analysed using the software program Visiopharm (Visiopharm 2020.08.1.8403; Visiopharm, Hoersholm, Denmark) to quantify the area of viral antigen expression in relation to the total area (area occupied by lung parenchyma) in the sections. This was used to compare the extent of viral antigen expression in the lungs between the different treatment groups. A first app was applied that outlined the entire lung tissue as ROI (total area). For this a Decision Forest method was used and the software was trained to detect the lung tissue section (total area). Once the lung section was outlined as ROI the lumen of large bronchi and vessels was manually excluded from the ROI. Subsequently, a second app with Decision Forest method was trained to detect viral antigen expression (as brown DAB precipitate) within the ROI.

qRT-PCR for viral load

Viral loads were quantified using the GoTaq® Probe 1-Step RT-qPCR System (Promega). For quantification of SARS-COV-2 the nCOV_N1 primer/probe mix from the SARS-CoV-2 (2019-nCoV) CDC qPCR Probe Assay (IDT) were utilised and murine 18S primers as described previously [25, 26].

Sequencing of SARS-CoV-2

Library preparation consisted of converting RNA to cDNA using LunaScript™ (Thermofisher), then amplified by reverse complement (RC)-PCR amplification (EasySeq™ SARS-CoV-2 Whole Genome Sequencing kit, Nimagen, Netherlands). This kit barcodes and ligates Illumina adapters in a single PCR reaction, with two

separate pools of primers (pools 1 and 2). After amplification, each amplicon library was pooled 1:1 before being cleaned with AmpliClean™ beads and quantification. The two pools were then added together and denatured. Finally, the denatured amplicon library was loaded into the NovaSeq cartridge (2 x 150 bp run).

Bioinformatics

Supplementary Fig. S2 provides an overview of the workflow used in this study. In short, raw paired end fastq files were inputted into the EasySeq pipeline to generate alignment files, vcf's and consensus sequences [34].Consensus sequences were inputted into Nextclade for lineage assignment and bam files were inputted into DiversiTools (https://github.com/josephhughes/DiversiTools) to assess minor variation. Sequencing data was analysed as previously described and statistical analysis and visualisation was performed in R [22]. Raw fastq files are available under SRA Project Accession: PRJNA886870. Code for analysis and figure generation is available at https://github.com/Hiscox-lab/viral-genomics-immunosupression-and-countermeasures.

Statistics

Graphs were prepared and statistics performed using Prism 10 (Graphpad Inc). *P* values were set at 95% confidence interval. A repeated-measures two-way ANOVA (Bonferroni post-test) was used for time-courses of weight loss; log-rank (Mantel-Cox) test was used for survival curve and Mann-Whitney *U* test for side-by-side comparisons. All differences not specifically stated to be significant were not significant ($p > 0.05$). For all figures, *$p < 0.05$.

Results and Discussion

Since the emergence of the Alpha VOC there has been discussion on the involvement of the immunocompromised host and the generation of variants [8, 35-39]. There are many case studies in the literature that follow SARS-CoV-2 evolution in immunocompromised hosts, however, little has been explored experimentally. In this study, mice were chemically immunocompromised with cyclophosphamide which is known to efficiently remove adaptive immunity in the form of B and T cells [40]. Additionally, therapeutic agents, molnupiravir and nirmatrelvir, were used independently and in combination to determine the effectiveness of these compounds in an immunocompromised model, and the impact of these compounds on viral sequence diversity.

Modelling an immunocompromised state in animal models in the context of SARS-CoV-2 is important for the consideration of countermeasures that may be utilised for humans who are considered vulnerable. Cyclophosphamide has been used previously to study the impact of immunosuppression in a hamster model [41-43], where intranasally infected hamsters with cyclophosphamide treatment before infection had prolonged weight loss and an inadequate neutralising antibody response to SARS-CoV-2. Distinct transcriptional profiles were identified between immunocompetent and immunosuppressed animals; however, the impact of antivirals or viral genome diversity was not investigated.

To investigate the frequency of genomic changes that occur in SARS-CoV-2 in the immune compromised or competent host in the presence or absence of antiviral drugs, K18-hACE2 transgenic mice were used as a model for severe SARS-CoV-2 infection in humans [44]. We have found that the pathological changes in the lungs in this model in many aspects resemble those in humans who have died of severe COVID-19 [26, 28, 29, 32, 33]. To mimic a host with compromised immunity, an experimental protocol was developed in which mice were exposed to cyclophosphamide [40] (Fig. 1, Table 1). Several anti-viral regimes in humans were simulated in the mouse model by giving a human equivalent dose of either molnupiravir (100 mg/kg), nirmatrelvir (500 mg/kg) or both in combination. This included prophylactic followed by therapeutic treatment. Mice were infected with 10^4 PFU of SARS-CoV-2.

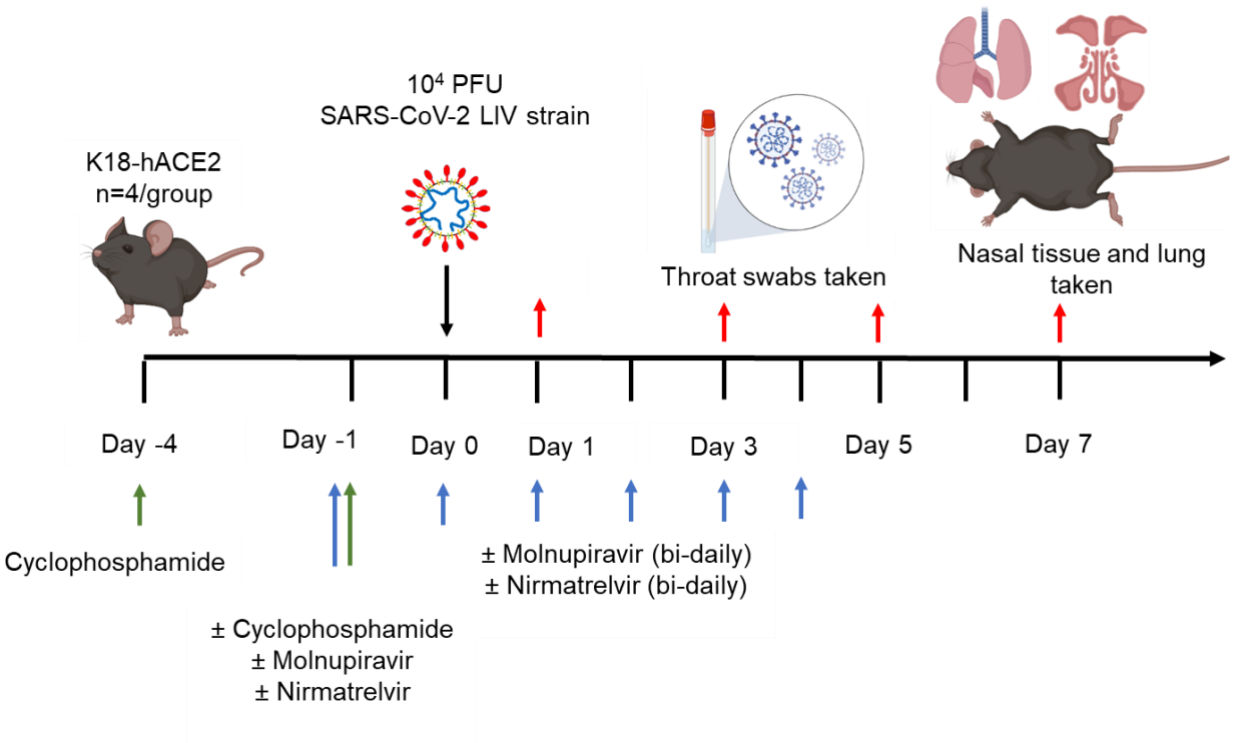

Figure 1. *Schematic diagram of the experimental design for infection of immune compromised K18-hACE2 mice with SARS-CoV-2 and evaluation of two antiviral drugs given at a human equivalent dose; molnupiravir, a broad acting compound causing error catastrophe, or nirmatrelvir which specifically targets the viral 3C-like protease. Cyclophosphamide was used at 100 mg/kg via the intraperitoneal route to immunosuppress mice. Molnupiravir was used at 100 mg/kg and* nirmatrelvir *at 500 mg/kg both via the oral route. Effects of infection and treatment were evaluated by measuring the weight of the mice daily, determining viral loads in sequential oral/throat swabs and at day 7 post-infection, and examining nose, brain and lung at day 7 post infection for any histological changes and the expression of SARS-CoV-2 nucleoprotein.*

245

246 **Table 1. Treatment groups for in vivo analysis**

Group	Treatment
1	Control (vehicle)
2	Cyclophosphamide
3	Molnupiravir
4	Cyclophosphamide + molnupiravir
5	Cyclophosphamide + nirmatrelvir
6	Cyclophosphamide + molnupiravir + nirmatrelvir

247

248

Treatment with Molnupiravir or Nirmatrelvir either individually or in combination provides recovery in immune compromised mice infected with SARS-CoV-2.

Cyclophosphamide treatment prior to SARS-CoV-2 infection of hACE2 mice led to a more pronounced early weight loss in comparison to immunocompetent mice, a phenomenon previously reported in hamsters [43]. This was not associated with earlier mortality than in vehicle treated immunocompetent mice, although in human, a delayed adaptive immune response has been shown to be associated with fatality in COVID-19 patients, which may have been observed over longer timeframes [45]. Daily weighing of the animals indicated that all groups lost body weight after day 1 (Fig. 2). We attribute this to aversion to eating as all therapies were applied by gavage. However, starting at day 3 all groups, except for mice exposed to cyclophosphamide, or mice exposed to cyclophosphamide and treated with molnupiravir, started to gain, or stabilise weight. By days 5 and 6 a clear pattern had emerged where all groups treated with molnupiravir or nirmatrelvir either individually or in combination had regained their starting weight. The exception to this were mice exposed to vehicle only (controls) or cyclophosphamide; these reached a humane end point on day 6 (Fig. 2). Comparison of survival curves again indicated that immune compromised animals treated either singly or in combination with each therapeutic went on to survive (Fig. 3).

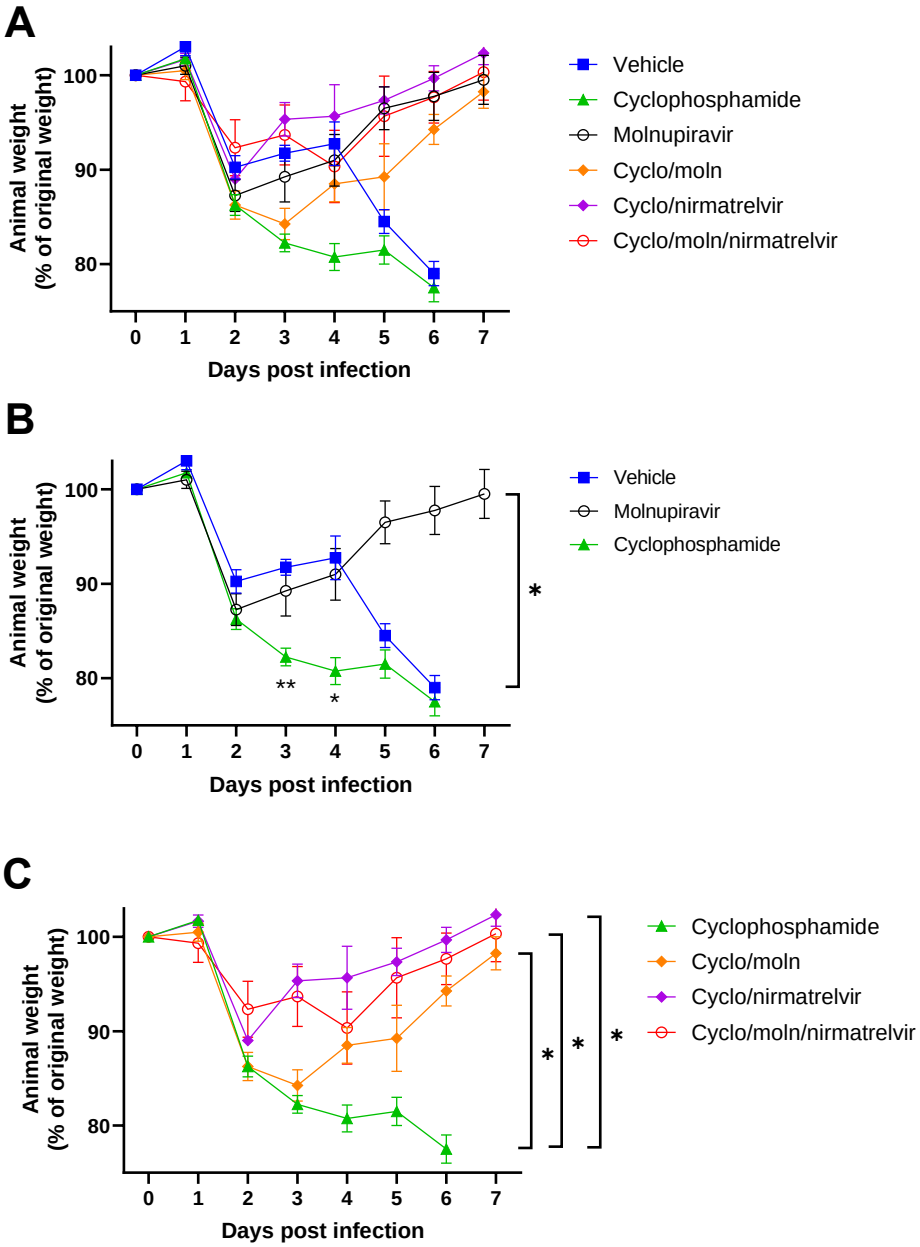

Figure 2: Treatment of SARS-CoV-2-infected immunocompromised mice leads to decreased weight loss. *K18-hACE2 mice were challenged intranasally with 10^4 PFU SARS-CoV-2 and their body weight monitored at indicated time-points (n = 4). Data represent the mean residual weight ± SEM. Comparisons were made using a repeated-measures two-way ANOVA (Bonferroni post-test). * Represents P < 0.05. Data from the same experiment were presented differently grouped in three separate graphs for clarity. (A) Curves for all groups. (B) Curves for vehicle, cyclophosphamide and molnupiravir groups. Asterisks below the curves represent * P < 0.05 and ** P < 0.01 between the cyclophosphamide and vehicle groups. (C) Curves for the groups treated with cyclophosphamide. Panels B and C were plotted using data shown in A but for added clarity.*

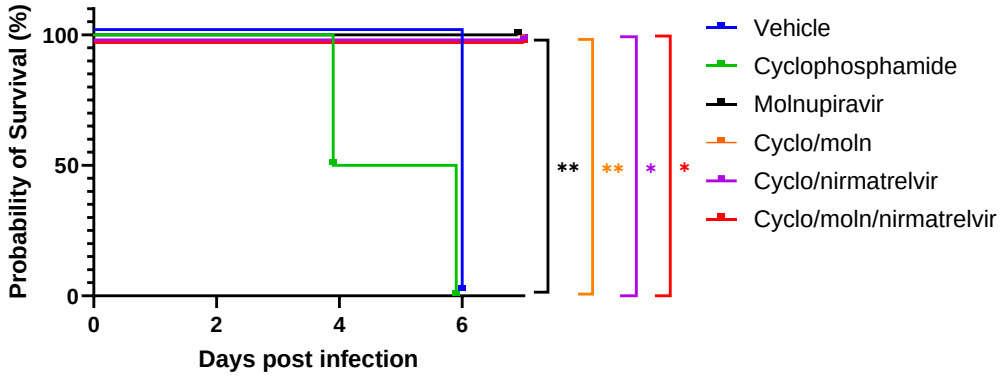

Figure 3: Treatment of SARS-CoV-2-infected mice leads to enhanced survival. *K18-hACE2 mice were challenged intranasally with 10^4 PFU SARS-CoV-2. Survival was assessed at indicated time points and significance determined using log rank (Mantel-Cox) test (n = 4).*

Viral load decreases in immune compromised mice treated with Molnupiravir or Nirmatrelvir either individually or in combination.

Viral load in terms of copy numbers of the SARS-CoV-2 genome were calculated for throat swabs during infection and compared to nasal tissue and lung tissue at the end of the experiment. The data indicated that for throat swabs on days 1 and 3 post-infection there was a significant decrease in viral load in animals treated with molnupiravir or nirmatrelvir either individually or in combination compared to untreated controls (Figure 4A). At day 3 there was a significant difference between both compounds used in combination and molnupiravir only (Figure 4A). No significant differences were observed between vehicle control and cyclophosphamide only groups.

Comparison of viral loads and titres in nasal and lung tissue respectively (Figure 4B and 4C, respectively) at day 7 post-infection reflected that there was a significantly lower viral load in animals treated with molnupiravir or nirmatrelvir either individually or in combination compared to untreated mice. However, nirmatrelvir treatment resulted in a greater decrease in viral load compared to molnupiravir. The molnupiravir/nirmatrelvir combination was also more effective at decreasing viral load than either drug alone, but this was only statistically significant in the case of molnupiravir vs the drug combination.

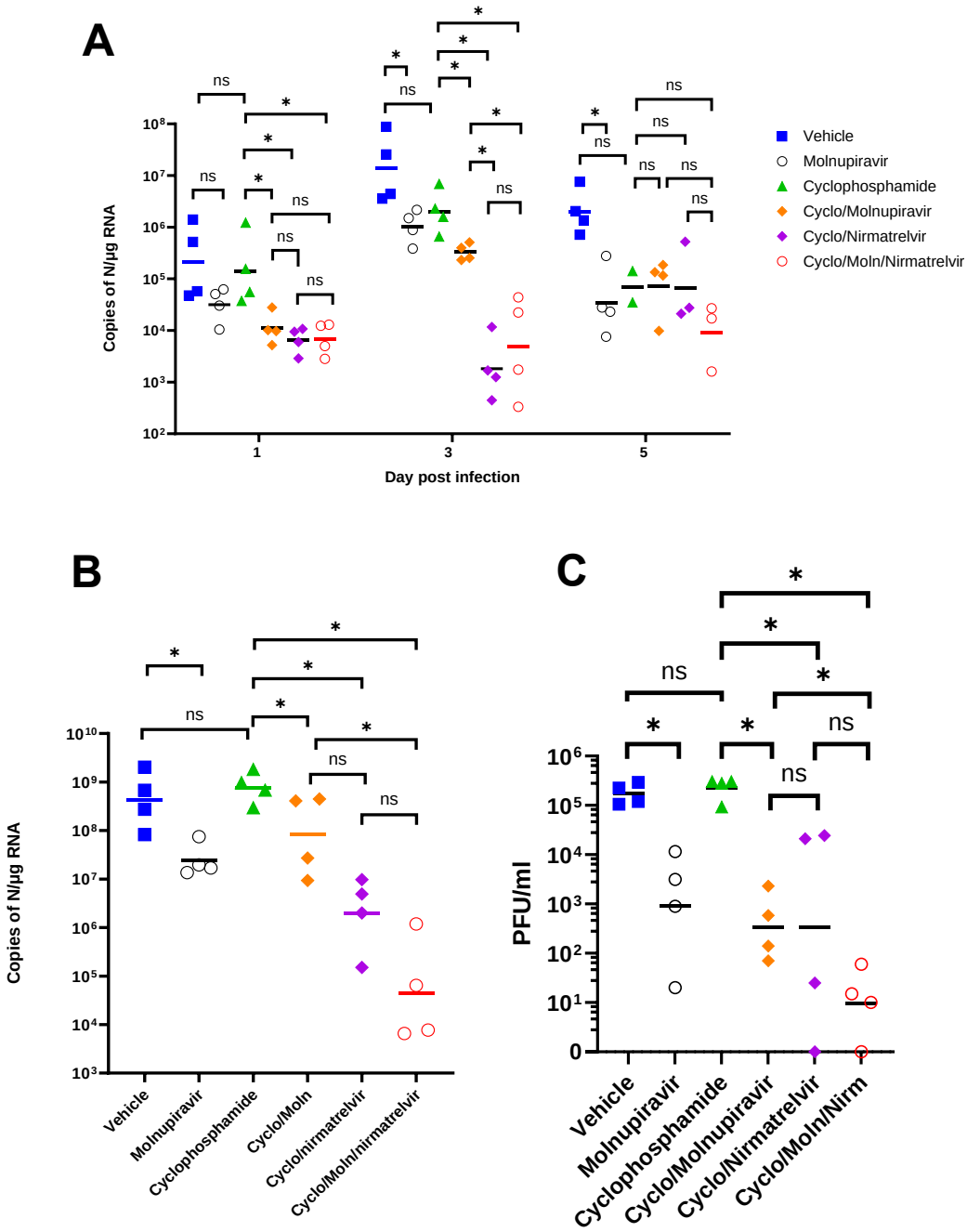

Figure 4. Viral loads in swabs and tissues. *K18-hACE2 mice were challenged intranasally with 10^4 PFU SARS-CoV-2 and treated as indicated (n = 4 per group). RNA extracted from oral/throat swabs and nasal tissue was analysed for virus RNA load using qRT-PCR and primers specific for the SARS-CoV-2 N gene. Assays were normalised relative to levels of 18S RNA. Lung tissue was analysed for live virus by plaque assay. Data for individual animals are shown with the median value represented by a black line. (A) Throat swabs; (B) nasal tissue; (C) lung tissue. Comparisons were made using two-way ANOVA (Bonferroni post-test) in panel A and Mann-Whitney U test (Panels B and C). * Represents $p < 0.05$.*

Treatment with molnupiravir or nirmatrelvir or both in combination results in marked reduction of pulmonary infection and inhibits viral spread to the brain.

The lung, nose and brain of all animals were examined for any histopathological changes and the expression of viral antigen by immunohistology, to determine whether treatment of the animals with molnupiravir and/or nirmatrelvir influenced the outcome of infection. The lungs of vehicle treated, immunocompetent animals showed the typical changes previously reported in K18-hACE2 mice infected with this virus strain [26], i.e. multifocal areas with pneumocyte degeneration, type II pneumocyte activation, mild neutrophil infiltration, and mild vasculitis, with a diffuse increase in interstitial cellularity and widespread SARS-CoV-2 antigen expression in alveolar epithelial cells (Fig. 5A). In mice that had received cyclophosphamide alone, the changes were very similar, but slightly less widespread, with some unaltered parenchyma and less extensive viral antigen expression (Fig. 5B). With molnupiravir treatment, both inflammatory processes and viral antigen expression were markedly decreased; indeed, SARS-CoV-2 antigen was only found in disseminated patches of alveoli with positive pneumocytes (Fig. 5C). With cyclophosphamide and molnupiravir treatment, the lung parenchyma was widely unaltered, and there were only small patches of inflammation and alveoli with viral antigen expression, respectively (Fig. 5D). These were further reduced in number and size in animals that had received cyclophosphamide and nirmatrelvir (Fig. 5E). Treatment with all three compounds, cyclophosphamide, molnupiravir and nirmatrelvir, resulted in widely unaltered lung parenchyma with no or minimal viral antigen expression (Fig. 5F). The morphometric analysis to quantify the extent of viral antigen expression in the lungs in the different groups of animals confirmed that the various antiviral treatment regimens significantly reduced the extent of lung infection (Figure S1).

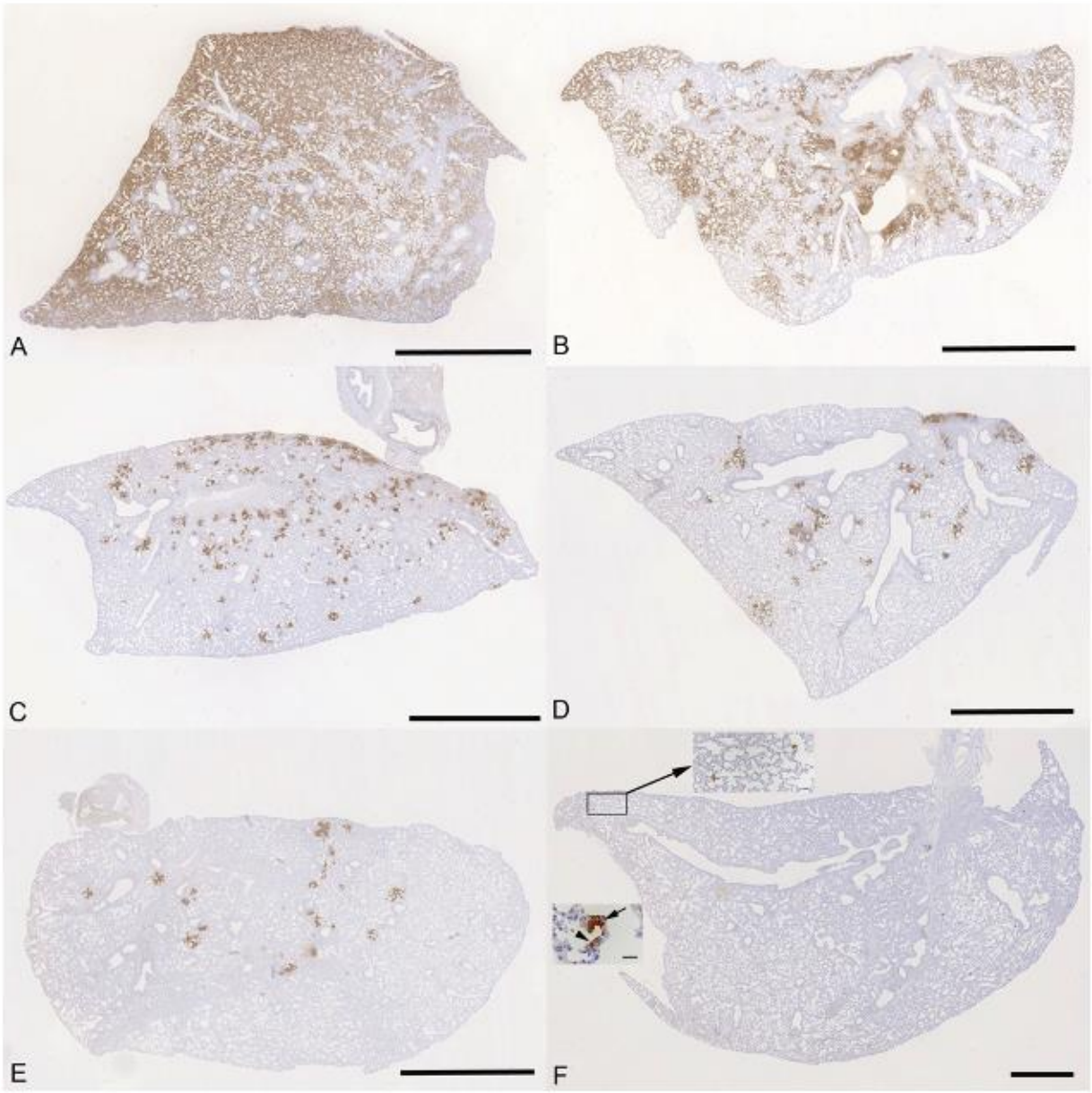

342

343 ***Figure 5****: K18-hACE2 mice were challenged intranasally with 10^4 PFU SARS-CoV-2 and*
344 *treated as indicated below (n = 4 per group). Immunohistology for the detection of viral antigen*
345 *in the lung at day 6 or 7 post infection. Sections from the formalin-fixed, paraffin embedded*
346 *left lung lobe were stained using anti-SARS-CoV nucleoprotein and counterstained with*
347 *hematoxylin. Representative images from the individual treatment groups are shown as*
348 *follows: A. vehicle; B. cyclophosphamide; C. molnupiravir; D. cyclophosphamide and*
349 *molnupiravir; E. cyclophosphamide and nirmatrelvir; F. cyclophosphamide, molnupiravir and*
350 *nirmatrelvir. Viral antigen expression is restricted to pneumocytes in a few individual alveoli*
351 *(higher magnifications in insets). Bars represent 2.5 mm (A-E), 1 mm (F) and 20 µm (F, insets).*

Examination of the heads using longitudinal sections (midline) revealed consistent and widespread infection of the brain in animals treated with the vehicle or with cyclophosphamide alone (Fig. 6A, B); this was associated with mild perivascular mononuclear infiltration in particular in the brain stem, as described before in K18-hACE2 mice infected with this virus strain [33]. In both groups of animals, immunohistology confirmed viral antigen expression in the respiratory and/or olfactory epithelium, in the latter with evidence of infection in olfactory sensory neurons (Fig. 6A, B). In the other groups, there was no evidence of viral infection of the brain (Fig. 6C-F), and viral antigen expression in the nasal mucosa was not seen or restricted to scattered individual epithelial cells. In vehicle control and cyclophosphamide mice, the nasal mucosa harboured viral antigen at this stage, in the respiratory epithelium and in the olfactory epithelium; in the latter it also appeared to be present in sensory neurons. Consequently, the virus had reached and spread widely in the brain where it was detected in neurons; the infection was associated with mild inflammatory response in particular in the brain stem, as described before in K18-hACE2 mice infected with this virus strain [26, 33]. After treatment with all three compounds, cyclophosphamide, molnupiravir and nirmatrelvir, the lung parenchyma was basically unaltered, with no or minimal viral antigen expression. In all groups of mice, viral antigen expression in the nasal mucosa was not seen or restricted to scattered individual epithelial cells and there was no evidence of viral infection of the brain, suggesting that the antiviral treatment blocked infection of the brain. Whether the latter is purely a consequence of reduced viral replication in the upper respiratory tract cannot be assessed in the present study; it does, however, appear likely.

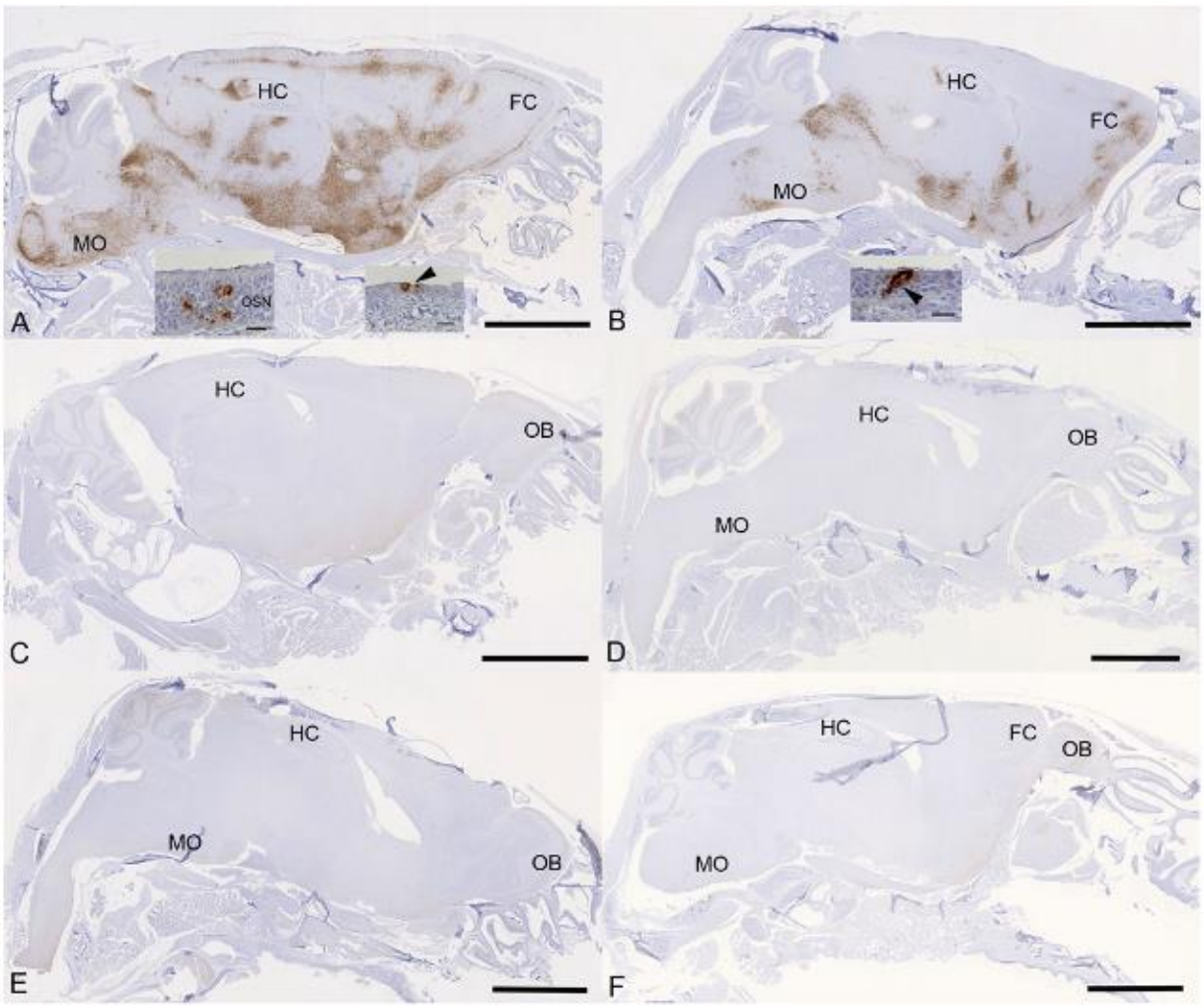

Figure 6*: K18-hACE2 mice were challenged intranasally with 10^4 PFU SARS-CoV-2 and treated as indicated below (n = 4 per group). Immunohistology for the detection of viral antigen in the brain and nose at day 6 or 7 post infection. Sections from formalin-fixed, decalcified and paraffin embedded heads after longitudinal sawing in the midline were stained using anti-SARS-CoV nucleoprotein, and counterstained with hematoxylin. Only small fragments of nasal mucosa were available for the examination, as the nasal turbinates had been sampled for PCR. Representative images from the individual treatment groups are shown as follows:* ***A****. Vehicle. There is widespread infection of the brain. The insets show infection of individual cells with the morphology of olfactory sensory neurons and epithelial cells in the olfactory epithelial layer (left inset) and individual respiratory epithelial cells in the nasal mucosa (arrowhead; right inset);* ***B****. Cyclophosphamide. There is widespread infection of the brain. The inset shows a group of positive epithelial cells/sensory neurons in the olfactory epithelial layer (arrowhead);* ***C****. Molnupiravir. There is no evidence of brain infection.* ***D****. Cyclophosphamide and molnupiravir. There is no evidence of brain infection.* ***E****. Cyclophosphamide and nirmatrelvir. There is no evidence of brain infection.* ***F****. Cyclophosphamide, molnupiravir and nirmatrelvir. There is no evidence of brain infection. Bars represent 2.5 mm (A-F) and 20 µm (A, B insets). FC – frontal cortex, HC – hippocampus, MO – medulla oblongata, OB – olfactory bulb, OSN - olfactory sensory neurons.*

Evaluation of dominant and minor variants in SARS-CoV-2

To determine the impact of immunosuppression on viral diversity, 116 RNA samples from swabs and tissue were sequenced and analysed using the EasySeq WGS protocol by Nimagen. alignment files and associated index files were inputted into DiversiTools to provide mutation data and outputs were analysed in R. Samples with less than 90% breadth of coverage were discarded for mutational analysis (n=12), as well as samples that returned bad or mediocre quality scores in nextclade (n=13). The samples that were excluded were associated with higher Ct values and later time points belonging in the nirmatrelvir treatment groups. Sequencing data from 89 samples were taken forward in the analysis (swab, n=50, tissue n=39, Supplementary Table S1).

The input virus contained 5 substitutions and 3 amino acid substitutions in comparison to the reference sequence and were thus not considered as changes during the analysis (Supplementary Table S2). The S: H655Y mutation was present in 76% of the genomes that passed QC at the dominant level and observed as a minor variant across all samples (Supplementary Fig. S3). This mutation has been reported previously as a spike adaptation to other species such as cats, hamsters, and mink [46-48] and of course has independently arisen in human lineages such as Omicron [49]. As this mutation was clearly associated with a species adaptation, it was disregarded for the evaluation of treatment and immune status driven mutations. The other mutations appear to be novel at the time of writing; however, no distinct group was associated with driving these mutations, and can be overall interpreted as a rare event. The sequences showing the highest number of mutations were sequences derived from tissue samples. Species specific adaptations were more frequently reported in the dataset than the immunocompromised and antiviral environments, putting the evolutionary pressures into perspective.

Molnupiravir increases the Ts/Tv ratio at the minor variant level in genomes derived from swabs

To further assess the impact of immunocompromising mice by cyclophosphamide, and the therapeutic agents molnupiravir and the nirmatrelvir, a minor variant analysis was conducted on samples derived from throat swabs. The average transition/transversion (Ts/Tv) ratio for SARS-CoV-2 genomes from each mouse and

the mean of each group was compared across cohorts. On day 1, an increase in Ts/Tv ration was observed in the molnupiravir cohort and the cyclophosphamide and molnupiravir cohort and had a p value < 0.05 when compared to the vehicle control and cyclophosphamide only groups (Fig. 7). The number of samples analysed for cyclophosphamide and nirmatrelvir only was too small for statistical analysis, however, the trend resembles that of vehicle and cyclophosphamide only. Likewise, the combined cyclophosphamide and molnupiravir and nirmatrelvir cohort only resembles one genome, however, the trend resembles that of other genomes with exposure to molnupiravir. The same is observed at day 3 of sampling, however, there is a significant difference between the mean Ts/Tv ratio between the molnupiravir only and cyclophosphamide and molnupiravir groups. Importantly, the Ts/Tv ratios between the vehicle control and cyclophosphamide only groups resemble each other. The proportion of base changes were also observed, with particular interest in the C to U and G to A transitions as previously seen in a phase II clinical trial [22] (Figure 8).

Further investigations are warranted to understand completely the role of immunocompromised individuals in the development of SARS-CoV-2 variants. It is more likely that immunodeficiency promotes viral persistence providing the virus more opportunity to replicate and introduce mutations. Molnupiravir, compared to nirmatrelvir, shows a stronger mutagenic effect in this model at the minor variant level, however, data is insufficient to make conclusions regards consensus level changes over the timeframes used in this study. When these therapies are used individually or in combination, there is successful depletion in viral load and animals recover from infection, whilst preventing infiltration into brain tissue. Given the concern of molnupiravir associated lineages in circulation [23], combination therapy may reduce this through more effective clearance of the virus [20], although this would need to be evaluated over time in a real-world setting as the mutational signatures were observed in the combined therapy group.

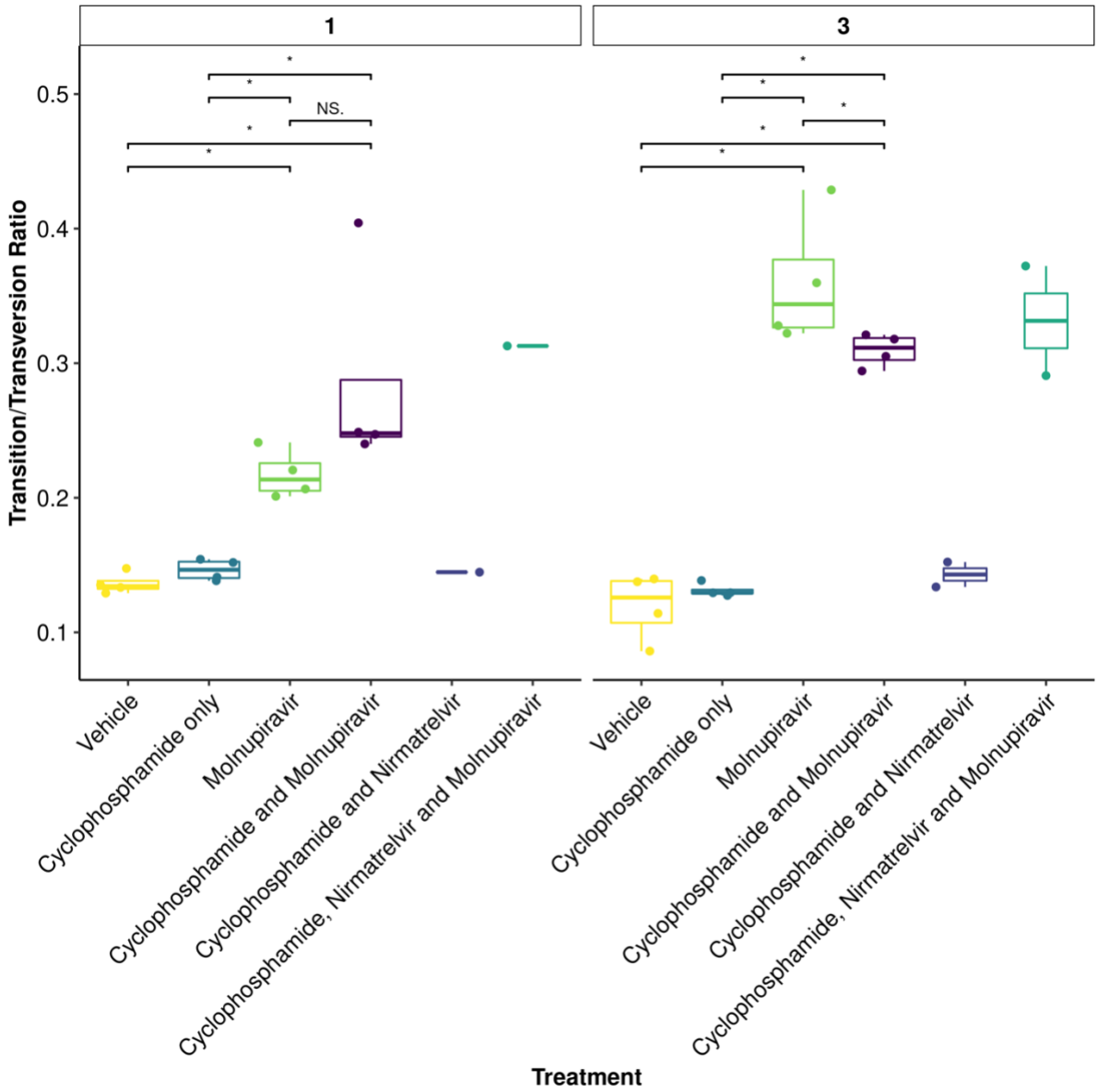

Figure 7: *The mean Ts/Tv ratio per genome plotted as boxplots. The plot is facetted by day post infection. Less genomes were recovered for cyclophosphamide and* nirmatrelvir *and cyclophosphamide,* nirmatrelvir *and molnupiravir, therefore statistical analysis returns the differences as non-significant. Trends can be concluded with caution. * Represents a P value <0.05 (Mann Whitney U test).*

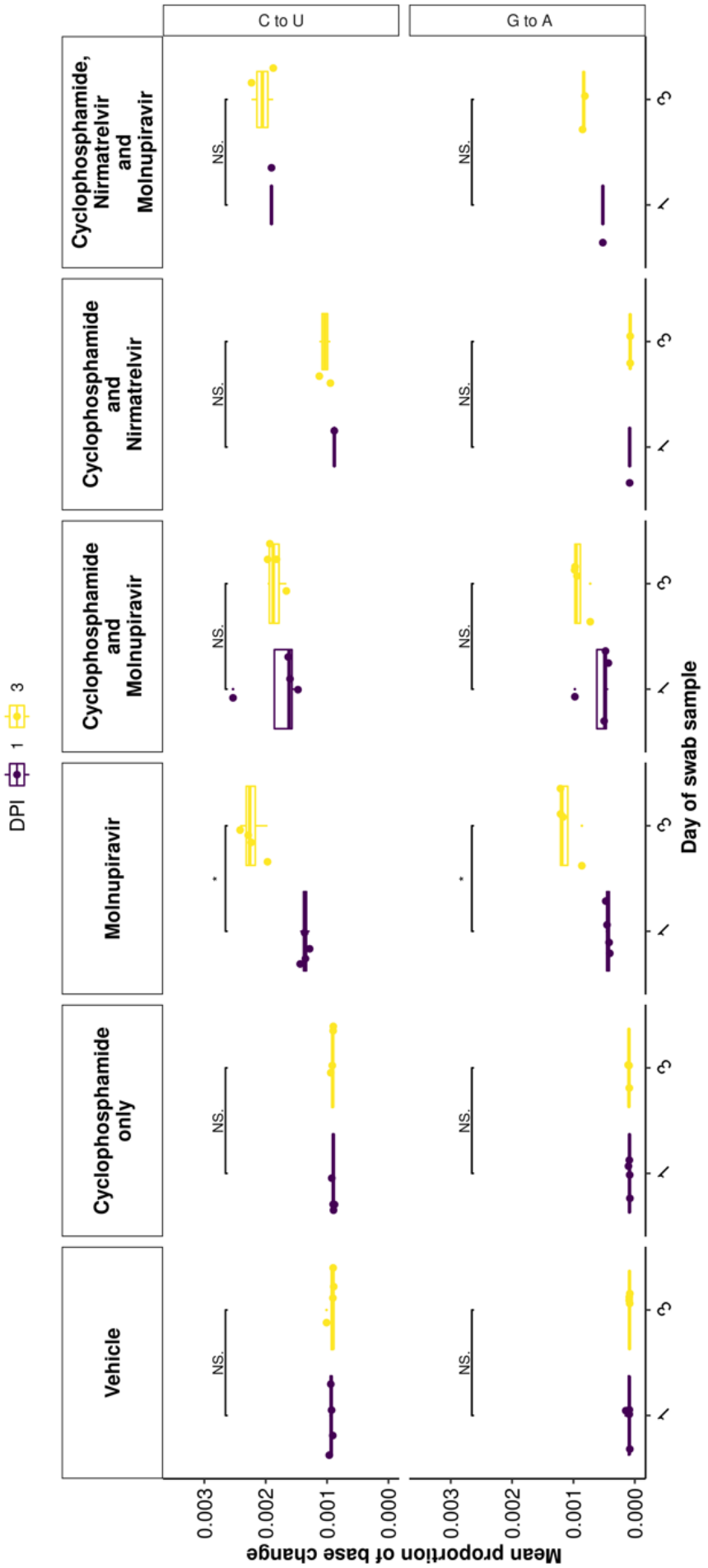

Figure 8: *C to U and G to A minor variation changes significantly increased between day 1 and day 3 post infection in the molnupiravir only group. A similar trend is observed between other groups including molnupiravir treatment, however, the change is not reported as significant. * represents a P value <0.05 (Mann Whitney U test).*

Acknowledgements

The authors are grateful to the technical staff at the Histology Laboratory, Institute of Veterinary Pathology, Vetsuisse Faculty, University of Zurich, for excellent technical support. JAH is a member of the ISARIC4C consortium (https://isaric4c.net/about/authors/), and we thankI them for the use of the SARS-CoV-2 isolate used in this study.

Funding

This work was funded by the MRC (MR/W005611/1) 'G2P-UK: A national virology consortium to address phenotypic consequences of SARS-CoV-2 genomic variation' and MR/Y004205/1 'The G2P2 virology consortium: keeping pace with SARS-CoV-2 variants, providing evidence to vaccine policy, and building agility for the next pandemic' (co-Is JPS and JAH) and funded in part by U.S. Food and Drug Administration Medical Countermeasures Initiative contract (75F40120C00085) to JAH. The article reflects the views of the authors and does not represent the views or policies of the FDA. Additionally, DNDi under the support by the Wellcome Trust (Grant ref: 222489/Z/21/Z to AO and JPS) through the 'COVID-19 Therapeutics Accelerator'. A.O. acknowledges funding by Wellcome Trust (222489/Z/21/Z), EPSRC (EP/R024804/1; EP/S012265/1) and National Institute of Health (NIH) (R01AI134091; R24AI118397). J.P.S. also acknowledges funding from the Medical Research Council (MRC) (MR/R010145/1, MR/W021641/1, PA6162_G2P2-2023), BBSRC (BB/R00904X/1; BB/R018863/1; BB/N022505/1) and Innovate UK (TS/W022648/1). A.K. received support from the Swiss National Science Foundation (SNSF; IZSEZ0 213289).

Transparency Declaration

A.O. is a director of Tandem Nano Ltd and co-inventor of patents relating to drug delivery. A.O. has been co-investigator on funding received by the University of Liverpool from ViiV Healthcare and Gilead Sciences in the past 3 years unrelated to COVID-19. A.O. has received personal fees from Gilead and Assembly Biosciences in the past 3 years, also unrelated to COVID-19. JPS has received funding from ENA respiratory Pty Ltd, Bicycle Tx Ltd, and Infex Therapeutics Ltd unrelated to this study. R.P.R. is an employee at TopMD Precision Medicine Ltd. No other conflicts are declared by the authors.

References

1. Moore SC, Penrice-Randal R, Alruwaili M et al. Amplicon-Based Detection and Sequencing of SARS-CoV-2 in Nasopharyngeal Swabs from Patients With COVID-19 and Identification of Deletions in the Viral Genome That Encode Proteins Involved in Interferon Antagonism. *Viruses* 2020; **12**.
2. McCarthy KR, Rennick LJ, Nambulli S et al. Natural deletions in the SARS-CoV-2 spike glycoprotein drive antibody escape. *bioRxiv* 2020: 2020.11.19.389916.
3. Korber B, Fischer WM, Gnanakaran S et al. Tracking Changes in SARS-CoV-2 Spike: Evidence that D614G Increases Infectivity of the COVID-19 Virus. *Cell* 2020; **182**: 812-27 e19.
4. Alruwaili M, Armstrong S, Prince T et al. SARS-CoV-2 NSP12 associates with TRiC and the P323L substitution acts as a host adaption. *Journal of virology* 2023; **97**: e0042423.
5. Goldswain H, Dong X, Penrice-Randal R et al. The P323L substitution in the SARS-CoV-2 polymerase (NSP12) confers a selective advantage during infection. *Genome Biology* 2023; **24**: 47.
6. Wang B, Goh YS, Prince T et al. Resistance of SARS-CoV-2 variants to neutralization by convalescent plasma from early COVID-19 outbreak in Singapore. *NPJ Vaccines* 2021; **6**: 125.
7. Suzuki R, Yamasoba D, Kimura I et al. Attenuated fusogenicity and pathogenicity of SARS-CoV-2 Omicron variant. *Nature* 2022; **603**: 700-5.
8. Corey L, Beyrer C, Cohen MS et al. SARS-CoV-2 Variants in Patients with Immunosuppression. *N Engl J Med* 2021; **385**: 562-6.
9. Avanzato VA, Matson MJ, Seifert SN et al. Case Study: Prolonged Infectious SARS-CoV-2 Shedding from an Asymptomatic Immunocompromised Individual with Cancer. *Cell* 2020; **183**: 1901-12 e9.
10. Young BE, Fong SW, Chan YH et al. Effects of a major deletion in the SARS-CoV-2 genome on the severity of infection and the inflammatory response: an observational cohort study. *Lancet* 2020; **396**: 603-11.
11. Aljabr W, Alruwaili M, Penrice-Randal R et al. Amplicon and Metagenomic Analysis of Middle East Respiratory Syndrome (MERS) Coronavirus and the Microbiome in Patients with Severe MERS. *mSphere* 2021; **6**: e0021921.
12. Chu DKW, Hui KPY, Perera R et al. MERS coronaviruses from camels in Africa exhibit region-dependent genetic diversity. *Proc Natl Acad Sci U S A* 2018; **115**: 3144-9.
13. El-Kafrawy SA, Corman VM, Tolah AM et al. Enzootic patterns of Middle East respiratory syndrome coronavirus in imported African and local Arabian dromedary camels: a prospective genomic study. *Lancet Planet Health* 2019; **3**: e521-e8.
14. Rottier PJ, Nakamura K, Schellen P et al. Acquisition of macrophage tropism during the pathogenesis of feline infectious peritonitis is determined by mutations in the feline coronavirus spike protein. *Journal of virology* 2005; **79**: 14122-30.
15. Licitra BN, Millet JK, Regan AD et al. Mutation in spike protein cleavage site and pathogenesis of feline coronavirus. *Emerg Infect Dis* 2013; **19**: 1066-73.
16. Vennema H, Poland A, Foley J et al. Feline infectious peritonitis viruses arise by mutation from endemic feline enteric coronaviruses. *Virology* 1998; **243**: 150-7.
17. Kipar A, Meli ML, Baptiste KE et al. Sites of feline coronavirus persistence in healthy cats. *The Journal of general virology* 2010; **91**: 1698-707.
18. Li P, Wang Y, Lavrijsen M et al. SARS-CoV-2 Omicron variant is highly sensitive to molnupiravir, nirmatrelvir, and the combination. *Cell Res* 2022; **32**: 322-4.

19. Gidari A, Sabbatini S, Schiaroli E et al. The Combination of Molnupiravir with Nirmatrelvir or GC376 Has a Synergic Role in the Inhibition of SARS-CoV-2 Replication In Vitro. *Microorganisms* 2022; **10**.
20. Hiscox JA, Khoo SH, Stewart JP et al. Shutting the gate before the horse has bolted: is it time for a conversation about SARS-CoV-2 and antiviral drug resistance? *J Antimicrob Chemother* 2021; **76**: 2230-3.
21. Szemiel AM, Merits A, Orton RJ et al. In vitro selection of Remdesivir resistance suggests evolutionary predictability of SARS-CoV-2. *PLoS Pathog* 2021; **17**: e1009929.
22. Donovan-Banfield Ia, Penrice-Randal R, Goldswain H et al. Characterisation of SARS-CoV-2 genomic variation in response to molnupiravir treatment in the AGILE Phase IIa clinical trial. *Nature Communications* 2022; **13**: 7284-.
23. Sanderson T, Hisner R, Donovan-Banfield Ia et al. A molnupiravir-associated mutational signature in global SARS-CoV-2 genomes. *Nature* 2023; **623**: 594-600.
24. Li P, de Vries AC, Kamar N et al. Monitoring and managing SARS-CoV-2 evolution in immunocompromised populations. *Lancet Microbe* 2022; **3**: e325-e6.
25. Bentley EG, Kirby A, Sharma P et al. SARS-CoV-2 Omicron-B.1.1.529 Variant leads to less severe disease than Pango B and Delta variants strains in a mouse model of severe COVID-19. *bioRxiv* 2021: 2021.12.26.474085.
26. Clark JJ, Penrice-Randal R, Sharma P et al. Sequential infection with influenza A virus followed by severe acute respiratory syndrome coronavirus 2 (SARS-CoV-2) leads to more severe disease and encephalitis in a mouse model of COVID-19. *bioRxiv* 2023: 2020.10.13.334532.
27. Gaynor KU, Vaysburd M, Harman MAJ et al. Multivalent bicyclic peptides are an effective antiviral modality that can potently inhibit SARS-CoV-2. *Nature Communications* 2023; **14**: 3583.
28. Russell CD, Valanciute A, Gachanja NN et al. Tissue Proteomic Analysis Identifies Mechanisms and Stages of Immunopathology in Fatal COVID-19. *Am J Respir Cell Mol Biol* 2021.
29. Dorward DA, Russell CD, Um IH et al. Tissue-Specific Immunopathology in Fatal COVID-19. *Am J Respir Crit Care Med* 2021; **203**: 192-201.
30. Patterson EI, Prince T, Anderson ER et al. Methods of Inactivation of SARS-CoV-2 for Downstream Biological Assays. *J Infect Dis* 2020; **222**: 1462-7.
31. Davidson AD, Williamson MK, Lewis S et al. Characterisation of the transcriptome and proteome of SARS-CoV-2 reveals a cell passage induced in-frame deletion of the furin-like cleavage site from the spike glycoprotein. *Genome Med* 2020; **12**: 68.
32. De Neck S, Penrice-Randal R, Clark JJ et al. The Stereotypic Response of the Pulmonary Vasculature to Respiratory Viral Infections: Findings in Mouse Models of SARS-CoV-2, Influenza A and Gammaherpesvirus Infections. Viruses 2023; 15(8) (Access Date Access 2023, date last accessed).
33. Seehusen F, Clark JJ, Sharma P et al. Neuroinvasion and Neurotropism by SARS-CoV-2 Variants in the K18-hACE2 Mouse. *Viruses* 2022; **14**.
34. Coolen JPM, Wolters F, Tostmann A et al. SARS-CoV-2 whole-genome sequencing using reverse complement PCR: For easy, fast and accurate outbreak and variant analysis. *Journal of Clinical Virology* 2021; **144**: 104993.
35. Avanzato VA, Matson MJ, Seifert SN et al. Case Study: Prolonged Infectious SARS-CoV-2 Shedding from an Asymptomatic Immunocompromised Individual with Cancer. *Cell* 2020; **183**: 1901-12.e9.

36. Burki T. The origin of SARS-CoV-2 variants of concern. *Lancet Infect Dis* 2022; **22**: 174-5.
37. Caccuri F, Messali S, Bortolotti D et al. Competition for dominance within replicating quasispecies during prolonged SARS-CoV-2 infection in an immunocompromised host. *Virus Evol* 2022; **8**: veac042.
38. Chen L, Zody MC, Di Germanio C et al. Emergence of Multiple SARS-CoV-2 Antibody Escape Variants in an Immunocompromised Host Undergoing Convalescent Plasma Treatment. *mSphere* 2021; **6**: e0048021.
39. Choi B, Choudhary MC, Regan J et al. Persistence and Evolution of SARS-CoV-2 in an Immunocompromised Host. *New England Journal of Medicine* 2020; **383**: 2291-3.
40. Peng KW, Myers R, Greenslade A et al. Using clinically approved cyclophosphamide regimens to control the humoral immune response to oncolytic viruses. *Gene Therapy* 2013; **20**: 255-61.
41. Schaecher SR, Stabenow J, Oberle C et al. An immunosuppressed Syrian golden hamster model for SARS-CoV infection. *Virology* 2008; **380**: 312-21.
42. Ramasamy S, Kolloli A, Kumar R et al. Comprehensive Analysis of Disease Pathology in Immunocompetent and Immunocompromised Hosts following Pulmonary SARS-CoV-2 Infection. *Biomedicines* 2022; **10**: 1343.
43. Brocato RL, Principe LM, Kim RK et al. Disruption of Adaptive Immunity Enhances Disease in SARS-CoV-2-Infected Syrian Hamsters. *J Virol* 2020; **94**.
44. Salzer R, Clark JJ, Vaysburd M et al. Single-dose immunisation with a multimerised SARS-CoV-2 receptor binding domain (RBD) induces an enhanced and protective response in mice. *FEBS Lett* 2021; **595**: 2323-40.
45. Legebeke J, Lord J, Penrice-Randal R et al. Evaluating the Immune Response in Treatment-Naive Hospitalised Patients With Influenza and COVID-19. *Front Immunol* 2022; **13**: 853265.
46. Escalera A, Gonzalez-Reiche AS, Aslam S et al. Mutations in SARS-CoV-2 variants of concern link to increased spike cleavage and virus transmission. *Cell Host Microbe* 2022; **30**: 373-87.e7.
47. Braun KM, Moreno GK, Halfmann PJ et al. Transmission of SARS-CoV-2 in domestic cats imposes a narrow bottleneck. *PLOS Pathogens* 2021; **17**: e1009373.
48. Mizuki Y, Keiko T, Youko H et al. SARS-CoV-2 Omicron spike H655Y mutation is responsible for enhancement of the endosomal entry pathway and reduction of cell surface entry pathways. *bioRxiv* 2022: 2022.03.21.485084.
49. Ou J, Lan W, Wu X et al. Tracking SARS-CoV-2 Omicron diverse spike gene mutations identifies multiple inter-variant recombination events. *Signal Transduction and Targeted Therapy* 2022; **7**: 138.